Journal of Materials Chemistry A

ROYAL SOCIETY OF CHEMISTRY

PAPER

View Article Online
View Journal | View Issue

Cite this: J. Mater. Chem. A, 2021, 9, 26028

UV curable stimuli-responsive coatings with antifogging and oil-repellent performances†

Jingyang Xu,‡[ab] Pengpeng Lu,‡[a] Li Wang,[b] Yong Fan,[b] Weijun Tian,*[a] Jianing Xu,[b] Jie Zhao,*[a] Luquan Ren[a] and Weihua Ming[c]

Received 15th September 2021
Accepted 4th November 2021

DOI: 10.1039/d1ta07934d

rsc.li/materials-a

Antifogging coatings prepared by highly hydrophilic/superhydrophilic strategies are susceptible to general oil contamination, hence readily losing their activities. Herein, a stimuli-responsive antifogging/oil-repellent coating with a delicate balance between hydrophilic and oleophobic components was prepared via a UV-assisted cross-linking method. Initially, different contents of acrylate monomers, including acrylic acid (AA), 1H,1H,2H,2H-tridecafluoro-*n*-octyl acrylate (TFOA), and 4-benzoylphenyl acrylate (BPA) were thermally polymerized to obtain a series of terpolymers, poly(AA-*co*-TFOA-*co*-BPA). Afterwards, poly(AA-*co*-TFOA-*co*-BPA) was covalently tethered to varied substrate surfaces (*i.e.*, glass slides, PC, PET, and PVC) through a UV triggered anchoring of BPA. Benefiting from the delicate balance between hydrophilic poly(AA) and oleophobic poly(TFOA), the resultant coating displays solvent sensitive stimuli-responsive wettability, driven by the encountered liquids with different surface tensions. Therefore, these coatings show excellent anti-fogging ability with ~90% light transmission, in a wide temperature range from −20 °C to 85 °C, meanwhile, the coatings also display remarkably high oil-repellence with an extremely low sliding angle for low tension liquids. These findings support the development of functional coatings that can highly maintain antifogging performances while effectively avoiding oil contamination in various imaging, medical and analytical applications.

Introduction

Fog droplets formed by moisture at condensation temperature would severely deteriorate the light transmittance of transparent substrates,[1] owing to the visible light scattering on the droplets,[2–8] which results in much inconvenience and even cause significant safety issues as fog largely decreases the clarity of mirrors, camera lenses, eyeglasses, windshields, periscopes, and other display devices in analytical and medical instruments.[9–15]

Till now, many strategies, referring to super-hydrophobic[14,16,17] and super-hydrophilic[5,18–23] surfaces, have been developed for eliminating the effect of fog droplets by rolling down from the surface or quickly spreading fog droplets into a continuous thin-film, so as to effectively avoid the light scattering.[12] Some superhydrophobic surfaces demonstrate reliable antifogging performance, but the light transmission tends to be compromised by its own micro-/nano-structured roughness.[24–27] On the other hand, these highly hydrophilic/super-hydrophilic surfaces are generally susceptible to oil contamination, hence readily losing their antifogging activities under certain conditions.[28–31]

It is still a challenge to prepare a functional surface with both hydrophilic and oil-repellent properties, largely because the hydrophilic and oleophobic properties, corresponding to high and low surface energy, respectively, are hard to be realized on a single surface.[32–35] To overcome this dilemma, some surfaces with both hydrophilic and oleophobic properties have been explored[29,32–34,36–39] through different strategies including layer by layer (LbL) assembly,[40,41] nanoparticle deposition[33,42] polymer brush grafting, *etc.*[7,28,43,44] Youngblood *et al.* reported that the block copolymers consisting of both polyethylene glycol and perfluorinate segments were grafted onto reactive substrates to form the coatings with stimuli-responsive antifogging/oil-repellent properties.[7] Sun *et al.* developed antifogging/oil-repellent surfaces by LbL assembly of hyaluronic acid (HA) and branched poly(ethylenimine) (bPEI), followed by immersion in aqueous solutions of perfluorooctanesulfonic acid potassium salt (PFOS) to obtain a surface with both hydrophilic and oleophobic performances.[36] Although these surfaces exhibited effective performances, the methods for the preparation of such surfaces are either confined to certain reactive substrates or involve tedious procedures, severely restricting their broad applications. Therefore, a simple and universal

[a]Key Laboratory of Bionic Engineering, Ministry of Education, Jilin University, Changchun 130022, China

[b]College of Chemistry, Jilin University, Changchun 130022, China

[c]Department of Chemistry and Biochemistry, Georgia Southern University, Statesboro, Georgia 30460, USA

† Electronic supplementary information (ESI) available. See DOI: 10.1039/d1ta07934d

‡ These authors contributed equally.

method that can endow various substrates with reliable antifogging/oil-repellent performances is still highly demanded.

Herein, we reported a stimuli-responsive antifogging/oil-repellent coating with the delicate balance between hydrophilic and oleophobic components *via* a facile UV-assisted cross-linking method. A series of terpolymers, poly(AA-*co*-TFOA-*co*-BPA) composed of AA, TFOA and BPA units, were prepared *via* a thermally triggered polymerization. Taking advantage of UV-triggered anchoring of BPA, the resultant poly(AA-*co*-TFOA-*co*-BPA) was firmly tethered to varied substrate surfaces (*e.g.*, glass slides, PC, PET, and PVC). Both the excellent antifogging properties and remarkable resistance against oil contamination were simultaneously possessed by the prepared coating, on which the fog droplets can be inhaled immediately while the oily liquids can be easily repelled, owing to the unique stimuli-responsive wettability stemming from hydrophilic poly(AA) and oleophobic poly(TFOA). The antifogging properties of the coatings with different ratios were systematically evaluated under both hot and cold-fogging conditions. The stimuli-responsive behavior and composition of the coating were examined by contact angle analysis, attenuated total reflectance Fourier-transform infrared spectroscopy (ATR-FTIR), and X-ray photoelectron spectroscopy (XPS). Moreover, the oil-repellent performance was also evaluated.

Experimental

Materials

The thermal initiator 2,2′-azobis(2-methylpropionitrile) (AIBN, 99%) was obtained from Aldrich and UV initiator 4-benzoylphenyl acrylate (4-BPA, 98%) was purchased from Macklin. Acrylate monomers including 1*H*,1*H*,2*H*,2*H*-tridecafluoro-*n*-octyl acrylate (stabilized with TBC) (TFOA, 97%) were obtained from Bidepharm. Acrylic acid (stabilized with MEHQ) (AA, 99%) was purchased from Mackin. 2-Propanol, *n*-decane, *n*-dodecane, *n*-hexadecane, THF, paraffin oil, octane, ethyl acetate, chloroform, toluene and 1,4-dioxane were provided by Energy Chemical Co, Ltd and used as received. Dimethylformamide (DMF) was purchased from Aladdin and dried over 4 Å molecular sieves. Red oil was provided by Macklin, Shanghai. All chemicals were analytical grade regents. Deionized water was used for all experiments.

Synthesis of terpolymer poly(AA-*co*-TFOA-*co*-BPA)

The terpolymer was prepared *via* a thermally triggered free radical polymerization, with azobisisobutyronitrile (AIBN) as an initiator. In detail, TFOA (0.04 g, 0.096 mmol), AA (2 g, 27.75 mmol), and BPA (0.0204 g, 0.081 mmol) were added to 10 mL DMF solution, followed by the addition of AIBN as the thermal initiator (0.0206 g, 1 wt% with respect to the total monomer mass). After being purged by argon for 20 min, the terpolymer was conducted at 75 °C for 8 h. The reaction was stopped by cooling water in an ice bath. The final terpolymer was purified by repeated dissolution in DMF and precipitation in petroleum ether. Similarly, different poly(AA-*co*-TFOA-*co*-BPA) were synthesized by changing the mass ratio of TFOA/AA, ranging from 0.04/2, 0.06/2, 0.1/2, 0.14/2, and 0.18/2, and were labelled as T-2, T-3, T-5, T-7, and T-9, respectively.

Coating preparation

Varied transparent substrates, involving glass slides (7.5 × 2.5 cm^2) (SAIL Brand, China), polycarbonate (PC), polyvinyl chloride (PVC), and polyethylene terephthalate (PET) were consecutively sonicated by using a KQ-100DV ultrasonic cleaning machine with ethanol for 30 min, dried by a high-purity nitrogen flow, and exposed to an air plasma atmosphere (PCE-6, Milliren Technologies, Inc.) for 180 s to completely clean the surfaces. A series of terpolymers (T-2, T-3, T-5, T-7, and T-9) were dissolved in DMF to obtain a homogeneous solution, respectively. The solution was spin-coated on clean substrates (glass slides, PC, PVC, and PET) at 1000 rpm for 15 s. After that, the coating was cured under UV irradiation with BPA as a photoinitiator in a UVP ultraviolet cross-linker apparatus (365 nm, 15 W) for 1800 s, and then dried in a vacuum oven at 75 °C for 12 h. The resultant coatings were denoted as C-2, C-3, C-5, C-7, and C-9, respectively, according to the related terpolymers used. The thickness of the obtained coatings was about 600 ± 200 nm determined by using a scanning electron microscope (SEM, JEOL JSM-IT500A), which was sufficient to ensure excellent antifogging performance (Fig. S1†).

The wettability of stimuli-responsive coatings

The wettability of the stimuli-responsive surface was examined using a contact angle (CA) goniometer (DSA, KRÜSSGMHBH, Hamburg 100), including static CAs and slide off angles (a tilting stage), mediated by *n*-hexadecane and water.

Fogging test

Fogging tests were carried out based on our previous trials.[4,11] The antifogging properties were conducted under both hot-vapor and cold-fog conditions. For the hot-vapor test, the glass slide covered by the coating was performed by holding the sample 10 cm above a hot water bath (85 °C) for 10 s. Digital photographs were taken immediately after the samples were removed and placed on top of a written letter under ambient conditions (~18 °C, relative humidity: 40–50%). For the cold-fog test, the sample was stored in a freezer at −20 °C for 20 min. In addition, light transmission data over the 400–700 nm range were collected on a UV-vis spectrophotometer (SP-1920, Shanghai Spectrum, China) during the fogging test. To further reveal the antifogging mechanism of coatings, the evolution of water contact angles on all the as-prepared coatings was monitored on a contact angle goniometer (DSA) and the time-dependent contact angles were collected every 4 s over an 80 s period.

Oil repellence test

Oil repellence of the as-prepared coatings was characterized by measuring the advancing angle (θ_{adv}), receding angle (θ_{rec}) and contact angle hysteresis (CAH) on a contact angle goniometer

(DSA), with approximately 10 μL liquid droplets (2-propanol, decane, *n*-dodecane, *n*-hexadecane, THF, paraffin oil, octane, ethyl acetate, chloroform, toluene, and 1,4-dioxane).

Adhesion force and abrasion resistance tests

The adhesive force of the coatings to the glass substrate was measured by two methods. (a) Cross-cut tape test (ISO-2049:2013) and (b) tensile test method (INSTRON-1121). As for method (a), briefly, a 100-cell grid containing 11 parallel and vertical lines were drawn out on a physical deposition coating (T-5 was deposited on the glass slide without UV radiation) and C-5 coating with a space of 1 mm between grid blades. Then a transparent adhesive tape (cat. 600, 3 M) was tightly placed upon the cuts on the coated area, followed by peeling off quickly. The scratched surfaces before and after peeling were observed using photographs and SEM. For method (b), the adhesion properties were quantitatively tested using a material testing machine at a rate of 5 mm min^{-1}. The abrasion resistance of the C-5 coating was assessed by cyclic sand abrasion, and each cycle includes a downward thrust motion followed by an upward thrust motion of the coating in the sand. The diameter of the sand was about 100–1000 μm.

Characterization

Surface chemical compositions were characterized by attenuated total reflectance Fourier-transform infrared spectroscopy (ATR-FTIR, Bruker Vertex 70) and X-ray photoelectron spectroscopy (XPS, ESCALAB 250 with a Al K_α X-ray source). H-nuclear magnetic resonance (^{1}H-NMR) spectra were collected on a Bruker Advance III 400 MHz spectrometer with DMSO-d_6 as the solvent. The number-average molecular weight (M_n) of the terpolymer was measured by using a gel permeation chromatograph (GPC), with a differential refractive index (RI) detector (Waters, 2410), and dimethylformamide (DMF) as the eluent (flow rate 1 mL min^{-1} at 80 °C), and polystyrene with the narrow-polydispersity was used as the calibration standard.

Results and discussion

Preparation of terpolymer poly(AA-*co*-TFOA-*co*-BPA)

A series of terpolymers poly(AA-*co*-TFOA-*co*-BPA) were synthesized by a convenient thermally triggered random polymerization (Fig. 1). Among these, T-5 with a TFOA/AA mass ratio of 0.1/2 was considered as the optimal sample for excellent antifogging/oil-repellent performance due to the balanced hydrophilic/hydrophobic contents, with M_n = 67 646 and M_w/M_n = 1.47, as determined from GPC (Fig. S2†). For the coating preparation, the existing BPA units in the terpolymers can serve as UV-curable groups; as a result, the covalently tethered coating can be obtained by a combination of the physical deposition of the terpolymers and UV irradiation. Among these, as "anchor groups", the BPA units in the terpolymer play a critical role in the stable coating formation on the substrate surface. Under UV irradiation, the BPA groups underwent an n–π* transition into a triplet state, resulting in the process of abstracting hydrogen atoms from the substrate.[45–49]

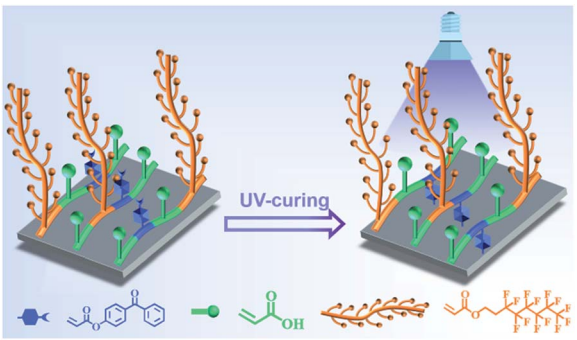

Fig. 1 Schematic illustration of the preparation of antifogging/oil-repellent coatings.

This abstraction, together with the subsequent generation of free radicals, facilitates the covalent attachment of the terpolymers to the substrate surfaces and form a "graft to" polymer (Fig. 1). In addition, the coating was monitored using UV-vis spectroscopy, where the decreasing absorbance of the BPA group spectrum from 300 to 350 nm was observed, ensuring the occurrence of photoinduced covalent binding to the glass slide surface (Fig. 2a). The structure of the prepared coatings was also confirmed from attenuated total reflection Fourier transform infrared (ATR-FTIR) spectroscopy spectra, as shown in Fig. 2b. The characteristic peak at 3280 cm^{-1} is attributed to the hydroxyl group, while the peaks at 1146–1240 cm^{-1} originate from $-CF_2-$ and $-CF_3$ in the PTFOA group, confirming that the as-prepared coatings have successfully adhered to the glass substrate. Moreover, the final detailed chemical composition of the terpolymer was determined *via* ^{1}H NMR in DMSO-d_6 (Fig. 2c). More detailed characterization studies of ATR-FTIR

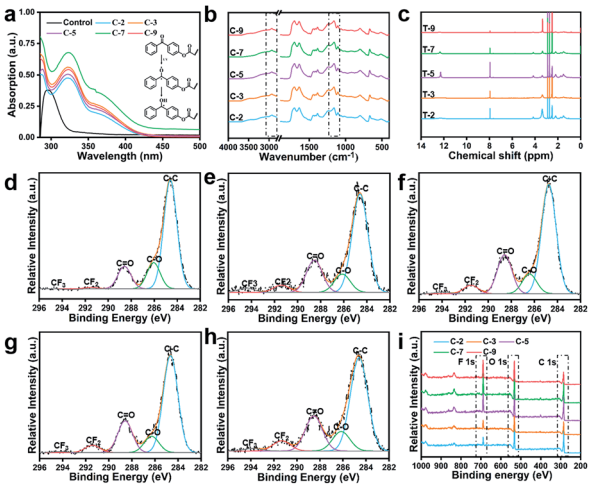

Fig. 2 (a) UV-vis spectra of the glass-coating as a function of irradiation time. (b) ATR-FTIR spectra of prepared terpolymer coatings. (c) ^{1}H NMR spectra of terpolymers poly(AA-*co*-TFOA-*co*-BPA). (d–h) High-resolution of C 1s for C-2, C-3, C-5, C-7 and C-9 coatings. (i) X-ray photoelectron spectroscopy (XPS) spectra of C-2, C-3, C-5, C-7 and C-9 coatings.

(Fig. S3†) and ^{1}H NMR (Fig. S4†) spectroscopy are described in the ESI.†

X-ray photoelectron spectroscopy (XPS) was used to examine the surface chemical components of different coatings. As shown in Fig. 2d–h, the high-resolution of C 1s peak for the terpolymer coatings was curve fitted to five peaks, C–C (~284.7 eV), C–O (~286.3 eV), C=O (~288.4 eV), –CF_2– (~291.4 eV) and –CF_3 (~293.3 eV). All major elements on the coating surfaces, C, O and F, are shown in Fig. 2i. The F element contents at the top surface of the samples with different TFOA/AA mass ratios (about 10 nm deep) were about 6.25%, 9.89%, 14.34%, 16.43% and 19.42%, respectively (Fig. 2i), which were about 5–7 times higher than the theoretical average F contents in the coatings, suggesting significant enrichment of TFOA on the coating surface. As proven by previous studies,[37,38,50] when the coating is exposed to air, the low surface energy chains (TFOA) orient towards the air interface while the high surface energy chains (AA) tend to remain beneath the outermost layer,[37] which will result in a significant surface enrichment of the fluoride segments in the coating, finally minimizing the free energy of the whole system. Consequently, the surface enrichment of fluoride in the resultant coatings would lead to excellent oil repellence.

The wettability of the stimuli-responsive surface

The stimuli-responsive behaviors of the terpolymer coatings were characterized by contact angle measurements. As shown in Fig. 3a, the water droplet was firmly pinned to the C-5 coating surface, even at a high tilt angle of 90°. However, the hexadecane droplet slid off the C-5 coating at a tilt angle of 5°, without any residue due to the significant enrichment of TFOA on the coating surface (Fig. 3b). The coating displays great wettability changes with the trigger of the water solvent. The C-5 coating showed the time-dependent water wetting properties, which initially demonstrated a WCA of ~59°, followed by a rapid decrease in WCA close to ~10° within 360 s (Fig. 3c). The terpolymer-based surfaces showing dual hydrophilic/oleophobic behavior could be termed solvent stimuli-responsive since they elicit a change of wettability in response to various solvent exposure.[7,28] As shown in Fig. 3d, contact angles (CAs) for water and hexadecane were collected from all as-prepared coatings. Obviously, the contact angles of water were always larger than those of hexadecane at the moment of contact; in fact, the relatively long water wetting time may be attributed to the high packing density of TFOA.[7,38] Densely arranged chains will likely show a slow response as the rearrangement process is hindered by spatial confinements. It is difficult for condensed water droplets to penetrate quickly through the hydrophobic PFOA layer into the coating. The solvent stimuli-responsive behavior reveals an antifogging/oil-repellent mechanism.

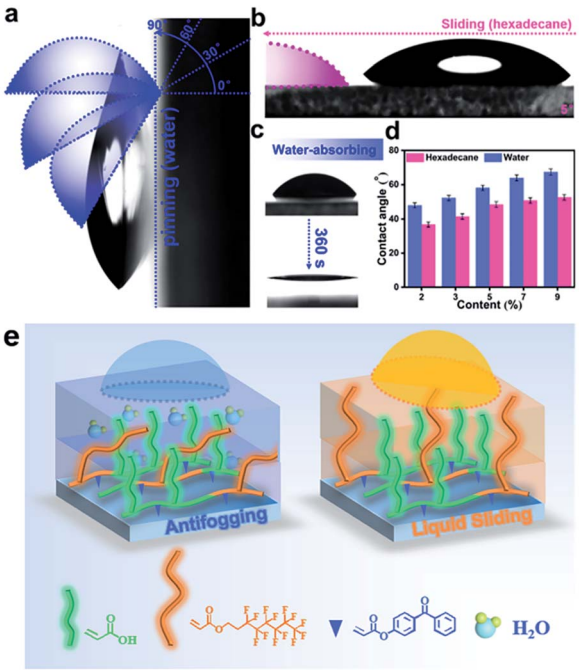

Fig. 3 (a–c) Static and dynamic wettability behaviour of water and hexadecane on the C-5 coating. (d) Static water and hexadecane contact angles of C-2, C-3, C-5, C-7, and C-9 coating surfaces. (e) Schematic of the mechanism of the antifogging and oil-repellent ability of the coatings.

As shown in Fig. 3e, when low surface energy solvents (*e.g.* oil and some organic solvents) come into contact with the surface, the surface enriched TFOA segments with low surface energy exhibit excellent oleophobic properties. Once the surfaces come into contact with water drops, the fluorinated constituents remain in a relatively mobile state and thus reorganize to allow for penetration of water molecules into the hydrophilic subsurface.[51] Generally, hydrophilic moieties provide favourable interactions with water. The penetration of water molecules would progress and wet the entire surface, eventually overcome fogging issues.[37]

Antifogging performance of the coating

Prior to the antifogging test, we evaluated light transmission of all coatings over the wavelength range of 400–700 nm. Compared to the bare glass, all coatings exhibited high light transmission for the whole visible light wavelength (~90%, Fig. 4a). Notably, the figure under the coated glass could be recognized clearly, which is comparable to that of the bare glass slide, indicating that the effect of the coating on the light transmission was negligible (Fig. S5†).

The antifogging performance of coatings was demonstrated with the hot-vapor and cold-fog methods. First, the optical images were recorded to observe light transmittance changes of coated/uncoated samples during both hot-vapor (Fig. 4b) and cold-fog tests (Fig. 4c). The bare glass slide fogged up immediately either by placing them above boiling water bath (85 °C for 10 s) or storing in a freezer at −20 °C for 20 min. In sharp contrast, there was no frost or fog formation at all for the C-5 coating, exhibiting the excellent antifogging performance under the same conditions, and suggesting the efficiency of fog inhibition. To further quantitatively evaluate the antifogging properties, the light transmission data over the wavelength

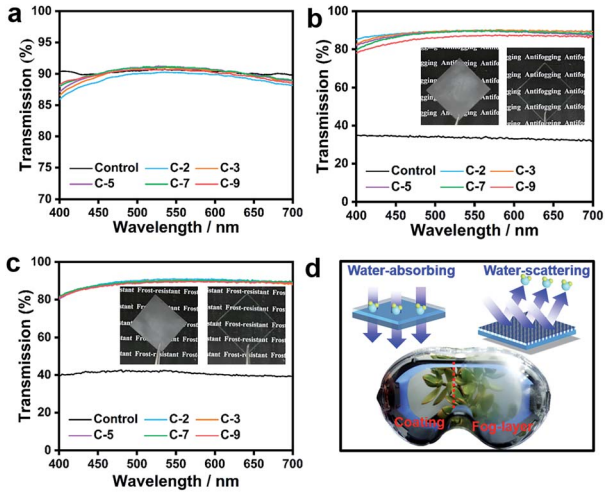

Fig. 4 (a) Light transmittance of the coatings and bare glass. The transmittance of the coatings and bare glass under the (b) hot-vapor and (c) cold-fog conditions. (d) Antifogging behavior of a pair of glasses with its left-hand lens covered with the C-5 coating.

range from 400 to 700 nm were collected. During the hot-vapor test, the light transmission of the bare glass decreased sharply to 40%, while sample coatings maintained high transmission (~90%, Fig. 4b). The antifogging performance of coatings was also evaluated, utilizing the cold-fog test by storing in a freezer at −20 °C for 20 min. Unsurprisingly, the bare glass fogged severely, seriously deteriorating the light transmission (~38%), whereas the as-prepared coatings demonstrated excellent anti-fogging properties (~90%, Fig. 4c), and the transmittance of the coatings slightly increased with the increase of the mass of AA. The results clearly suggested that the hydrophilic AA units played an active role in the antifogging performance by immediately inhaling the condensed water to obtain a fog free coating surface (Fig. 4d).

To further reveal the antifogging mechanism, time-dependent evolution of the WCA on the coatings was measured over an 80 s period under ambient conditions (~18 °C, 40–50% relative humidity) (Fig. 5a). Unlike a typical superhydrophilic antifogging surface (CA approaching 0°), all the coatings exhibited initial WCA above 40° (Fig. 5a). The result reinforced the recent findings in the references that an effective antifogging coating does not have to be superhydrophilic.[11,41] In addition, the WCA on all coatings decreased much more rapidly than on the bare glass slide, indicating that some water had likely diffused into the coating. Thus, no large light-scattering water domain would be formed, ensuring excellent light transparency. We also simultaneously monitored the change in the basal diameter of a water droplet on the coating surface. No obvious change in the basal diameter was observed on the bare glass slide over the 80 s period; however, the droplet basal diameter increased on all the as-prepared coatings to various extents (Fig. 5b), depending on the TFOA content in the coating. C-2 had the largest expansion in the droplet basal diameter (35.6%), followed by C-3 (31.8%), C-5 (29.0%), C-7 (27.7%) and C-9 (25.9%).

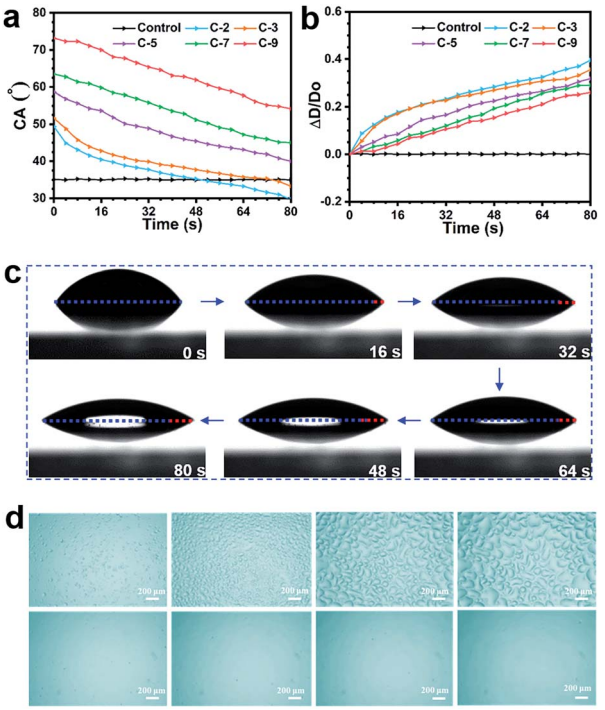

Fig. 5 (a) Various water contact angle values on different coatings within the 80 s time period. (b) Basal diameter changes of the water droplet on different coatings over the 80 s period expressed as $\Delta D/D_0$, where $\Delta D = D - D_0$ and D_0 is the basal diameter at $t = 0$ s (all the data were the average of three times recorded in a 4 s interval). (c) Optical images of the water droplets on the C-5 coating during the water absorption process. (d) Photos of the C-5 coating under the fluorescence microscope in the hot vapor test (the interval between each photo was 10 s).

These results also suggested that water had diffused into the coating, causing the expansion of the droplet basal area on the coating surface (Fig. 5c). Obviously, the introduction of a higher amount of hydrophobic TFOA led to a decrease in the water-absorbing capability (less water expansion, *e.g.* C-9) of the coatings, which was consistent with the antifogging properties of the coatings we discussed above. The excellent anti-fogging performance of the C-5 coating was further tested by using a fluorescence microscope. As shown in Fig. 5d, there were many water droplets on the bare glass slide; however, no water droplets could be observed on the C-5 coating, which verified the outstanding anti-fogging ability.

Oil repellence of the coating

A static CA does not accurately describe the repellence of the coating surface against liquid droplets.[52,53] Recent findings on the preparation of oil-repellent surfaces have demonstrated that minimizing the contact angle hysteresis (CAH) is the key criterion for oleophobic effectiveness.[54,55] For a given surface, a droplet of the liquid has advancing angle (θ_{adv}), receding angle (θ_{rec}), and the difference ($\Delta\theta = \theta_{adv} - \theta_{rec}$) is defined as the contact angle hysteresis (CAH). Therefore, to properly characterize the oil-repellent properties, θ_{adv}, θ_{rec}, and CAH values were collected. The hexadecane CAH values of the coatings with

different TFOA concentrations are presented in Fig. 6a. All coatings exhibited high CAs (θ_{adv}, θ_{rec}) and low CAHs (C-2, C-3, C-5, C-7, and C-9 showed $\Delta\theta = 11.5° \pm 0.67°$, $8.4° \pm 1.33°$, $4.4° \pm 0.86°$, $2.5° \pm 1.30°$, and $2.2° \pm 1.52°$, respectively). The low CAHs indicated that the coatings exerted low adhesive forces for hexadecane, exhibiting excellent oil-repellent properties. The CAH decreases with the increase of the fluoride concentration, indicating low surface energy TFOA is vital for enhancing surface oil-repellence. As expected, the low TFOA content (C-2, C-3) could not provide excellent oil-repellent performance, whereas the high TFOA content could slightly affect the anti-fogging properties of the coatings. For environmental considerations, the as-prepared coatings with less fluoride still provided excellent oil repellence performance to meet the requirements. Therefore, the C-5 coating was adopted as the optimal antifogging/oil-repellent coating. Time-sequence images of the 10 μL hexadecane droplet could easily slide off with a tilt angle of 5°. To demonstrate the oleophobicity of the C-5 coating intuitively, photos were taken to record the sliding process of paraffin oil (15 s) and hexadecane (6 s) on the C-5 coating as the substrate was tilted at 15° (Fig. 6b). To further evaluate the oil-repellent ability of the coatings, some organic solvents, including 2-propanol, decane, *n*-dodecane, *n*-hexadecane, THF, paraffin oil, *n*-octane, ethyl acetate, chloroform, 1,4-dioxane, and toluene with various surface tensions, were taken as the probe liquids. All liquids exhibited the CAH lower than 10° on the C-5 coating and indicated the excellent oil-repellent properties (Fig. 6c). In addition, in Mov. S1,† these liquid droplets slid off the C-5 coating readily without any residue. Notably, the coatings could repel most commercial paraffin oils with high viscosity, presenting their potential values. We also applied the antifogging/oil-repellent coating to the various substrates, (*e.g.* PC, PET and PVC). Hexadecane as the probe liquid exhibited on all pre-treated substrates exhibited excellent oil-repellent properties (Fig. S6†).

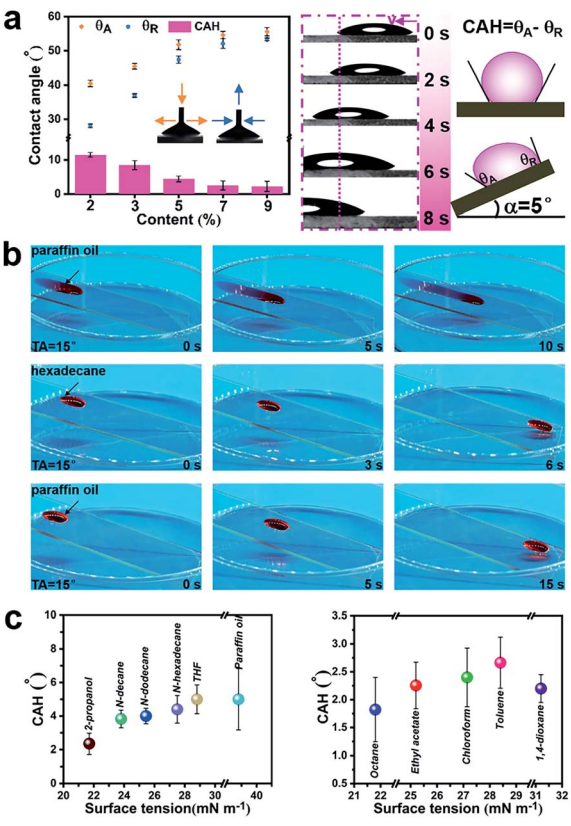

Fig. 6 (a) θ_{adv}, θ_{rec} and CAH ($\Delta\theta$) of the hexadecane on the sample coatings; time-sequence images of the 10 μL hexadecane droplet sliding on the C-5 coating with a tilt angle (TA) of 5°. (b) Surface liquid repellence of C-5 against hexadecane and paraffin oil (dyed by oil red, tilted angle of 15°). (c) CAH of different organic liquids on glass slides coated with C-5 coatings.

Adhesion force and abrasion resistance tests

For the cross-cut tape test, the C-5 coating possessed more excellent adhesion performance, as compared to the physically deposited coating. Fig. S7† shows photographs of both physical deposition and C-5 coating before and after the cross-cut tape test. Prior to the tape peeling, for the physical deposition coating, the edges of the cuts were rough, and then some parts of the coating fell off after being peeled by tape. In contrast, the cut edges of the C-5 coating were smooth without any cracks before the tape peeling test. After being peeled by tape, no obvious difference was found on the coating surface and the edges of the cuts were intact with no coating detachment; these results were further confirmed by the SEM investigation. Moreover, the adhesion of the C-5 coating was also quantitatively evaluated by using a material test machine (INSTRON-1121). A sharp enhancement (~4.7 MPa) in the tensile strength for the C-5 coating was observed, ~46% increase in the tensile strength value, as compared to that of the physically deposited coating (~3.2 MPa) (Fig. S8†), which evidently indicated the increased adhesion force of the C-5 coating on the substrate. Abrasion resistance is also a critical factor for the coatings in practical applications, and the cyclic sand abrasion test is a commonly used method to evaluate the stability of the coating.[40,52] After 30 cycles of sand abrasion, the C-5 coating showed no sign of damage while maintaining the remarkable antifogging/oil-repellent properties (Fig. S9†).

Conclusions

In summary, by a facile UV-crosslinking technology based on a terpolymer with BPA as the reaction anchor, a bifunctional antifogging/oil-repellent coating can be conveniently formed on various substrates including both inorganic and polymeric materials. The antifogging/oil-repellent behavior primarily originated from the delicate hydrophilic/hydrophobic balance of terpolymers. Owing to the high water-absorbing capacity of PAA, the coating exhibit excellent antifogging properties. Meanwhile, the coatings have outstanding oil-repellence with low CAH to various oils and organic liquids, stemming from the perfluoroalkyl chains on the coating. Moreover, the coating also maintained excellent mechanical stability, as verified by the cross-cut tape test, tensile test and abrasion resistance. We believe that this type of functional coating may find unique

applications where both antifogging and oil-repellent properties are desired.

Author contributions

Jingyang Xu and Pengpeng Lu should be considered joint first authors.

Conflicts of interest

There are no conflicts to declare.

Acknowledgements

The authors gratefully acknowledge the financial support by the Science and Technology Development Plan Project of Jilin Province (No. 20190201155JC and 20190201278JC), the Young and Middle-aged Technology Innovation Leading Talents and Team Projects of Science and Technology Development Plan of Jilin Province (20200301013RQ), the Natural Science Foundation of Guangxi Province (No. 2020GXNSFAA238041), the Pre-research Foundation of Equipment Key Laboratory (Grant No. JCKY 61420052005), the Scientific Research Foundation of the Education Department of Jilin Province (Grant No. JJKH20190145KJ), and the Interdisciplinary Integration and Innovation Project of Jilin University for Young Scholar.

Notes and references

1 J. Yoon, M. Ryu, H. Kim, G. N. Ahn, S. J. Yim, D. P. Kim and H. Lee, *Adv. Mater.*, 2020, **32**, e2002710.
2 W. Wang, P. Lu, Y. Fan, L. Tian, S. Niu, J. Zhao and L. Ren, *Chem. Eng. J.*, 2019, **378**, 122173.
3 Z. Han, X. Feng, Z. Guo, S. Niu and L. Ren, *Adv. Mater.*, 2018, **30**, e1704652.
4 J. Zhao, P. Lu, L. Song, L. Tian, W. Ming and L. Ren, *Colloids Surf., A*, 2020, **585**, 124160.
5 Y. Yang, T. Sun, F. Ma, L. F. Huang and Z. Zeng, *ACS Appl. Mater. Interfaces*, 2021, **13**, 3377–3386.
6 M. Tzianou, G. Thomopoulos, N. Vourdas, K. Ellinas and E. Gogolides, *Adv. Funct. Mater.*, 2020, **31**, 2006687.
7 J. A. Howarter and J. P. Youngblood, *Adv. Mater.*, 2007, **19**, 3838–3843.
8 C. Tao, S. Bai, X. Li, C. Li, L. Ren, Y. Zhao and X. Yuan, *Prog. Org. Coat.*, 2018, **115**, 56–64.
9 K. Feng, L. Peng, L. Yu, Y. Zheng, R. Chen, W. Zhang and G. Chen, *ACS Appl. Mater. Interfaces*, 2020, **12**, 27632–27639.
10 Y. Wang, L. Yao, T. Ren and J. He, *J. Colloid Interface Sci.*, 2019, **540**, 107–114.
11 J. Zhao, L. Ma, W. Millians, T. Wu and W. Ming, *ACS Appl. Mater. Interfaces*, 2016, **8**, 8737–8742.
12 J. Zhao, A. Meyer, L. Ma and W. Ming, *Chem. Commun.*, 2013, **49**, 11764–11766.
13 H. Qi, C. Zhang, H. Guo, W. Zheng, J. Yang, X. Zhou and L. Zhang, *ACS Appl. Mater. Interfaces*, 2019, **11**, 24504–24511.
14 Z. Sun, T. Liao, K. Liu, L. Jiang, J. H. Kim and S. X. Dou, *Small*, 2014, **10**, 3001–3006.
15 S. Bai, X. Li, Y. Zhao, L. Ren and X. Yuan, *ACS Appl. Mater. Interfaces*, 2020, **12**, 12305–12316.
16 G. B. Darband, M. Aliofkhazraei, S. Khorsand, S. Sokhanvar and A. Kaboli, *Arabian J. Chem.*, 2020, **13**, 1763–1802.
17 T. Mouterde, G. Lehoucq, S. Xavier, A. Checco, C. T. Black, A. Rahman, T. Midavaine, C. Clanet and D. Quere, *Nat. Mater.*, 2017, **16**, 658–663.
18 L. Daeyeon, R. Michael F and C. Robert E, *Nano Lett.*, 2006, **6**, 2305–2312.
19 L. Ning, K. Jun, R. Yufang, L. Xue and L. Chunsheng, *Ceram. Int.*, 2021, **47**, 18743–18750.
20 X. Liu, X. Du and J. He, *ChemPhysChem*, 2008, **9**, 305–309.
21 X. Ligang and H. Junhui, *ACS Appl. Mater. Interfaces*, 2012, **4**, 3293–3299.
22 W. S. Y. Wong, N. Nasiri, A. L. Rodriguez, D. R. Nisbet and A. Tricoli, *J. Mater. Chem. A*, 2014, **2**, 15575–15581.
23 X. Wang, S. Li, J. Huang, J. Mao, Y. Cheng, L. Teng, Z. Chen and Y. Lai, *Chem. Eng. J.*, 2021, **409**, 128228.
24 Y. Shao, W. Du, Y. Fan, J. Zhao, Z. Zhang and L. Ren, *Chem. Eng. J.*, 2022, **427**, 131718.
25 X. Xie, S. Li, X. Wang, J. Huang, Z. Chen, W. Cai and Y. Lai, *Chem. Eng. J.*, 2021, **426**, 131245.
26 Q. Li and Z. Guo, *Nanoscale*, 2019, **11**, 18338–18346.
27 L. Chen, Z. Guo and W. Liu, *ACS Appl. Mater. Interfaces*, 2016, **8**, 27188–27198.
28 J. A. Howarter and J. P. Youngblood, *Macromol. Rapid Commun.*, 2008, **29**, 455–466.
29 J. Yang, Z. Zhang, X. Xu, X. Zhu, X. Men and X. Zhou, *J. Mater. Chem.*, 2012, **22**, 2834–2837.
30 C. Chen, D. Weng, A. Mahmood, S. Chen and J. Wang, *ACS Appl. Mater. Interfaces*, 2019, **11**, 11006–11027.
31 Y. Pan, S. Huang, F. Li, X. Zhao and W. Wang, *J. Mater. Chem. A*, 2018, **6**, 15057–15063.
32 J. Li, L. Yang, H. Liu, G. Li, R. Li, Y. Cao and H. Zeng, *ACS Appl. Mater. Interfaces*, 2020, **12**, 45266–45273.
33 F. Li, Z. Wang, S. Huang, Y. Pan and X. Zhao, *Adv. Funct. Mater.*, 2018, **28**, 1706867.
34 C. Huanjie, X. Zhiguang, Z. Tao, L. Xiaomin, W. Zhu and Z. Yan, *J. Colloid Interface Sci.*, 2021, **594**, 122–130.
35 D. K. Owens and R. C. Wendt, *J. Appl. Polym. Sci.*, 1969, **13**, 1741–1747.
36 F. Xu, X. Li, Y. Li and J. Sun, *ACS Appl. Mater. Interfaces*, 2017, **9**, 27955–27963.
37 H. Chi, Z. Xu, Y. Ma, T. Tang, T. Zhang and Y. Zhao, *Adv. Sustainable Syst.*, 2020, **4**, 2000049.
38 E. P. Milnes-Smith, C. A. Stone and S. Perkin, *Chem. Commun.*, 2020, **56**, 2877–2880.
39 J. Lu, Z. Gao, T. Xu, X. Zhu, X. Miao, Y. Song, G. Ren and X. Li, *ACS Appl. Mater. Interfaces*, 2020, **12**, 49138–49145.
40 L. Yu, G. Y. Chen, H. Xu and X. Liu, *ACS Nano*, 2016, **10**, 1076–1085.
41 H. Lee, J. B. Gilbert, F. E. Angile, R. Yang, D. Lee, M. F. Rubner and R. E. Cohen, *ACS Appl. Mater. Interfaces*, 2015, **7**, 1004–1011.
42 X. Li, J. Liu, R. Qu, W. Zhang, Y. Liu, H. Zhai, Y. Wei, H. Hu and L. Feng, *Nat. Commun.*, 2021, **12**, 80.

43 H. Guo, T. Xu, J. Zhang, W. Zhao, J. Zhang, C. Lin and L. Zhang, *Chem. Eng. J.*, 2018, **351**, 409–417.
44 T. Sato, G. J. Dunderdale and A. Hozumi, *ACS Appl. Polym. Mater.*, 2021, **3**, 1395–1405.
45 S. L. Chin, R. Xiao, B. G. Cooper, N. Varongchayakul, K. Buch, D. Kim and M. W. Grinstaff, *J. Appl. Polym. Sci.*, 2016, **133**, 43930.
46 Y. Leixiao, H. Yong, C. Chong, S. Christoph, N. P.-L. Michael, W. Qiang and H. Rainer, *ACS Appl. Mater. Interfaces*, 2017, **9**, 44281–44292.
47 L. Xiaojie, W. Kan, Z. Qiong, J. Priyesh, B. M. O'Kelly, L. Bowen, H. H. Chieh, C. Sharon A, H. Jonathan, R. Buddy D and J. Shaoyi, *ACS Appl. Mater. Interfaces*, 2020, **12**, 41026–41037.
48 X. Lin, K. Fukazawa and K. Ishihara, *ACS Appl. Mater. Interfaces*, 2015, **7**, 17489–17498.
49 A. Schneider-Chaabane, V. Bleicher, S. Rau, A. Al-Ahmad and K. Lienkamp, *ACS Appl. Mater. Interfaces*, 2020, **12**, 21242–21253.
50 G. Zhang, J. Jiang, Q. Zhang, F. Gao, X. Zhan and F. Chen, *Langmuir*, 2016, **32**, 1380–1388.
51 T. Sato, G. J. Dunderdale and A. Hozumi, *Langmuir*, 2020, **36**, 7439–7446.
52 Y. Wang, Y. Fan, P. Zhang, L. Tian, J. Xu, S. Niu, L. Ren, J. Zhao and W. Ming, *Prog. Org. Coat.*, 2021, **154**, 106170.
53 D. F. Cheng, C. Urata, M. Yagihashi and A. Hozumi, *Angew. Chem., Int. Ed.*, 2012, **51**, 2956–2959.
54 M. Liu, Z. Wang, P. Liu, Z. Wang, H. Yao and X. Yao, *Sci. Adv.*, 2019, **5**, eaaw5643.
55 L. Wang and T. J. McCarthy, *Angew. Chem., Int. Ed.*, 2016, **55**, 244–248.